Applied Catalysis B: Environmental 140–141 (2013) 598–607

Contents lists available at SciVerse ScienceDirect

Applied Catalysis B: Environmental

journal homepage: www.elsevier.com/locate/apcatb

# Size effect induced activity enhancement and anti-photocorrosion of reduced graphene oxide/ZnO composites for degradation of organic dyes and reduction of Cr(VI) in water

Yanhui Zhang[a,b], Zhang Chen[a,b], Siqi Liu[a,b], Yi-Jun Xu[a,b,*]

[a] State Key Laboratory Breeding Base of Photocatalysis, College of Chemistry and Chemical Engineering, Fuzhou University, Fuzhou 350002, PR China
[b] College of Chemistry and Chemical Engineering, New Campus, Fuzhou University, Fuzhou 350108, PR China

ARTICLE INFO

*Article history:*
Received 30 January 2013
Received in revised form 23 April 2013
Accepted 28 April 2013
Available online 4 May 2013

*Keywords:*
Reduced graphene oxide
ZnO
Photostability
Size and synergetic effect
Interfacial contact

ABSTRACT

The composites of reduced graphene oxide/ZnO (RGO/ZnO) with different particles size of ZnO have been prepared *via* a facile solvothermal reaction of graphene oxide (GO) and ZnO in an ethanol-water solvent. It is found that the RGO/ZnO-S1 composite with ZnO particle size of 20–100 nm exhibits the enhanced photoactivity toward degradation of organic dyes and reduction of heavy metal ions Cr(VI) in water as compared to the bare ZnO-S1 sample under UV light irradiation. However, the RGO/ZnO-S2 composite with ZnO particle size of 50–500 nm shows decreased photoactivity as compared to bare ZnO-S2. The recycled photoactivity testing shows that, for RGO/ZnO-S1, the photocorrosion of ZnO-S1 is efficiently inhibited by the hybridization with RGO whereas the case is not for RGO/ZnO-S2. A collection of characterization techniques disclose that the smaller particles size for RGO/ZnO-S1 than that for RGO/ZnO-S2 leads to a more interfacial contact and a chemical bonding between RGO and ZnO-S1, thereby resulting in enhanced photoactivity and efficient anti-photocorrosion as observed for RGO/ZnO-S1. Furthermore, the possible reaction mechanism for degradation of dyes and reduction of Cr(VI) over RGO/ZnO-S1 has also been studied. Our results suggest that the semiconductor particles size has an important effect on the photocatalytic performance of RGO/semiconductor composites photocatalysts. The hybridization of RGO with ZnO in an appropriate manner is able to significantly inhibit the well-known photocorrosion of semiconductor ZnO. It is anticipated that this work would enrich the applications of RGO/semiconductor photocatalysts in environment purification.



## 1. Introduction

Heterogeneous photocatalysis by semiconductor materials has been attracting a great deal of interest owing to its universal application especially in degradation of pollutants (dyes, bacteria, and volatile organic pollutant), water splitting to hydrogen, photocatalytic reduction (e.g., $CO_2$ photo-reduction to solar fuels, and heavy metal ions reduction), and selective organic transformations to fine chemicals (e.g., alcohols to aldehydes, and C—H activation) [1–18]. Among the abundant semiconductor materials, $TiO_2$-based and ZnO-based composites materials have been extensively investigated as active semiconductor photocatalysts [16–21]. However, compared with the relative stability of $TiO_2$-based composites, ZnO with higher photocatalytic efficiency for liquid-phase degradation of organic dyes than $TiO_2$ holds the drawback of photocorrosion effect during light irradiation, which causes the decrease in photocatalytic activity and stability [22–30].

A lot of research interest has been devoted to designing ZnO-based composite materials, aiming to enhance the photocatalytic activity and inhibition of photocorrosion of semiconductor ZnO [25–30]. Several methods have been developed to improve its photostability, including surface organic coating of ZnO, embedding ZnO into perfluorinated ionomer membranes, formation of surface complex, and surface hybridization of ZnO with graphite-like carbon such as monolayer polyaniline and fullerenes $C_{60}$ [25–30]. Notably, Zhu et al. once reported that $C_{60}$-hybridized ZnO could enhance activity and photostability for the degradation of methylene blue under ultraviolet (UV) light irradiation [30]. Therefore, analogous phenomenon could also be observed for the composites of ZnO and graphene (GR), another carbon allotrope and rising star in materials science. In fact, during the past few years, GR-based composite photocatalysts have been attracting increased research attention, aiming to utilize the excellent electron conductivity and 2D structure of GR for target applications in solar energy

* Corresponding author at: State Key Laboratory Breeding Base of Photocatalysis, College of Chemistry and Chemical Engineering, Fuzhou University, Fuzhou 350002, PR China. Tel.: +86 591 83779326.
*E-mail address:* yjxu@fzu.edu.cn (Y.-J. Xu).

0926-3373/$ – see front matter © 2013 Elsevier B.V. All rights reserved.
http://dx.doi.org/10.1016/j.apcatb.2013.04.059

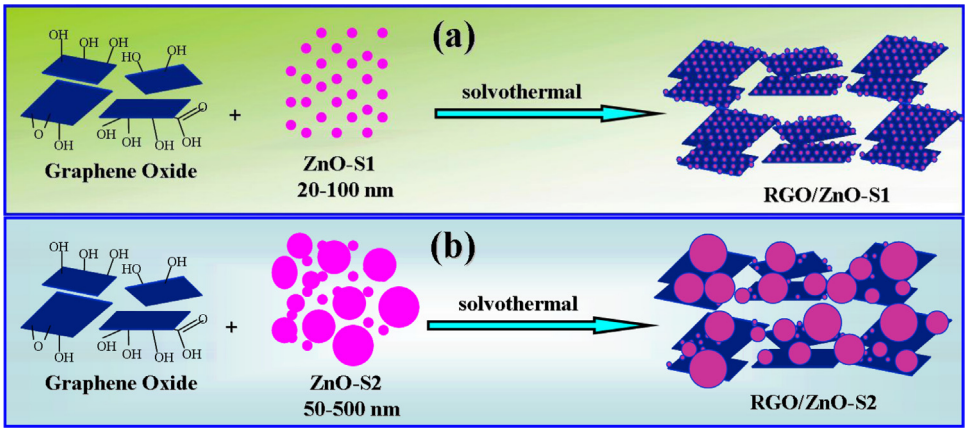


**Scheme 1.** Flow chart for preparation of RGO/ZnO-S1 composites (a) and RGO/ZnO-S2 composites (b) by a solvothermal treatment in the solvent of ethanol-water.

conversion [31–55]. In most cases, because GR is often obtained by the reduction of graphene oxide (GO) regarding synthesis of GR-based composites photocatalysts, it is often called reduced GO (RGO) [31].

To date, RGO-semiconductor or -metal (e.g., $TiO_2$, ZnO, $WO_3$, $SnO_2$, $BiVO_4$, $Bi_2WO_6$, ZnS, $ZnFe_2O_4$ and Au) composite photocatalysts have been demonstrated to be a viable strategy for achieving an enhanced photocatalytic activity toward nonselective degradation of pollutants in both liquid and gas phases [31–51]. Several investigations on the RGO/ZnO composites have been reported in the fields of degradation of dyes, solar cells, reduction of Cr(VI), sensor, bacteria destruction and supercapacitors [41,42,57–81]. Notably, research works on RGO/ZnO composite photocatalysts are mainly focused on emphasizing the enhanced photoactivity of ZnO owing to the hybridization of ZnO with RGO [41,42,58–73]. However, several significant and fundamental issues still remain unclear so far. First, can the addition of RGO into the matrix of ZnO effectively improve the photostability of semiconductor ZnO, namely inhibiting the well-known photocorrosion of ZnO, besides the enhanced photoactivity? If so, in what manner should RGO integrate with ZnO particles? Second, it has been unaddressed regarding the size effect of ZnO nanoparticles in RGO/ZnO composites on the photocatalytic activity [41,42,58–73]. Third, the detailed reaction mechanism, i.e., the role of photogenerated radical species in photocatalytic process driven by RGO/ZnO composites photocatalysts, has been unclear yet.

From the viewpoint of synthesis of efficient RGO-semiconductor composites toward achieving a more sufficient interfacial contact between RGO and semiconductor, the soft integration of RGO with a soluble precursor of semiconductor in a wet chemistry process is more advantageous over the hard integration of RGO with solid semiconductor particles because the soft integration method is able to harness the surfactant-like "structure-directing" role of GO, which provides a 2D platform for nucleation and growth of soluble precursor into corresponding semiconductor particles in a wet chemistry process [54]. However, with regard to this synthesis approach, it is difficult for us to focus on primarily studying the particles size effect of semiconductor on the photocatalytic activity of RGO-semiconductor composites. In this regard, the hard integration of RGO and solid semiconductor particles with different size distribution, which can be directly obtained by choosing different sized hard semiconductor particles before assembling with RGO, offers us a simple choice to mainly concentrate on investigating the size effect of semiconductor particles on the photocatalytic activity of RGO-semiconductor composites because, during the hard integration process, the size of semiconductor particles can be maintained almost the same as that of the original solid semiconductor particles [39,42,53].

Against this background, we herein report the synthesis of RGO/ZnO composites with different particle size of ZnO via a facile solvothermal approach. We investigate the photocatalytic activity and stability of RGO/ZnO composites toward degradation of organic dyes and reduction of Cr(VI) in an aqueous phase, and the underlying photocatalytic reaction mechanism. It is found that the RGO/ZnO-S1 composite with ZnO particle size of 20–100 nm exhibits the enhanced photocatalytic activity as compared to bare ZnO-S1, but the RGO/ZnO-S2 composite with ZnO particle size of 50–500 nm shows decreased photocatalytic activity. Furthermore, the efficient inhibition of photocorrosion is observed for RGO/ZnO-S1 whereas the case is not for RGO/ZnO-S2, signifying the important effect of particles size of ZnO on the synergetic interaction between ZnO and RGO sheet, which thus influences the photocatalytic performance of RGO/ZnO composites photocatalyst. In addition, the possible reaction mechanism has been studied by the electron spin resonance (ESR) spectra and controlled experiments using radical scavengers techniques.

## 2. Experimental

### 2.1. Preparation of photocatalysts

Graphene oxide (GO) was prepared based on a well-established approach for the exfoliation of oxidized graphite as reported earlier from our group [53–56]. Two types of zinc oxide (ZnO) powder is used. One is the nanoparticulate ZnO (particle size: 20–100 nm, namely ZnO-S1, supplied from Aladdin Co. Ltd). The other is commercial ZnO (particle size: 50–500 nm, namely ZnO-S2, also supplied from Aladdin Co. Ltd). To synthesize RGO/ZnO composites with different addition ratios of GO, a simple solvothermal method was used, which allows for the sufficient reduction of GO to reduced graphene oxide (RGO) [53,82]. The preparation process is illustrated in Scheme 1. Typically, the as-prepared GO with the desired weight addition was dispersed in a 26 mL of deionized water and 13 mL of anhydrous ethanol solution completely by ultrasonication, and then 0.2 g ZnO was added and kept stirring for 2 h to obtain a homogeneous suspension. After that, it was transferred to 50 mL Teflon-sealed autoclave and maintained at 393 K for 12 h. Next, the products were cooled to room temperature and recovered by filtration, washed by water, and fully dried at 333 K in an oven. The final RGO/ZnO-S1 and RGO/ZnO-S2 composites with different weight addition ratios of RGO, namely 1, 5, 10, and 20% RGO/ZnO-S1, were thus obtained.

### 2.2. Characterization of photocatalysts

The crystal phase properties of the samples were determined by X-ray diffraction (XRD, Philip X' Pert Pro MPP) using a Cu Kα radiation (λ = 1.5418 Å) in the 2θ ranging from 5° to 80° with a scan rate of 0.08 per second. The optical properties of the samples were analyzed by UV–vis diffuse reflectance spectroscopy (DRS) using a UV–vis spectrophotometer (Cary 500, Varian), in which $BaSO_4$ was employed as the internal reflectance standard. Field-emission scanning electron microscopy (FE-SEM) was used to characterize the morphology of the samples on a FEI Nova NANOSEM230 spectrophotometer. The Fourier transformed infrared spectroscopy (FT-IR) was performed on a Nicolet Nexus 670 FT-IR spectrophotometer at a resolution of 4 $cm^{-1}$. The particles size distribution was performed using a Nano measurer software. The photoluminescence (PL) spectra were obtained using an Edinburgh Analytical Instrument PLS920 system.

The radical species were detected by electron spin resonance (ESR) spectrometer on a Bruker EPR A300 instrument. In detail, the sample (5 mg) was dispersed in 0.5 mL of purified solvent (deionized water or anhydrous ethanol), into which 25 μL of 5,5-dimethyl-l-pyrroline-N-oxide (DMPO)/solvent (deionized water or anhydrous ethanol) solution (1:10, v/v) was added. The mixture was oscillated to obtain a well-blending suspension. The UV light irradiation source was a 300 W Xe arc lamp system equipped with a band-pass light filter (λ = 365 ± 15 nm), which is the same light source as for the photoactivity test. The parameters for the ESR spectrometer were as follows: center field = 3512 G, microwave frequency = 9.86 GHz, and power = 2.01 mW.

The electrochemical analysis was carried out in a conventional three-electrode cell using a Pt plate and an Ag/AgCl electrode as the counter electrode and reference electrode, respectively. The electrolyte was 0.2 M $Na_2SO_4$ aqueous solution without additive (pH 6.8). The working electrode was prepared on indium-tin oxide (ITO) glass that was cleaned by sonication in ethanol for 30 min and dried at 353 K. The boundary of ITO glass was protected using Scotch tape. The 10 mg sample was dispersed in 1 mL of ethanol by sonication to get slurry. The slurry was spread onto the pretreated ITO glass. The working electrode was dried overnight under ambient conditions. Then, the Scotch tape was unstuck, and the uncoated part of the electrode was isolated with epoxy resin. The exposed area of the working electrode was 0.25 $cm^2$. The UV light irradiation source was a 300 W Xe arc lamp system equipped with a band-pass light filter (λ = 365 ± 15 nm), which is the same light source as for the photoactivity test. The photocurrent measurements were taken on a BAS Epsilon workstation without bias. The electrochemical impedance spectroscopy (EIS) experiments were conducted on a Precision PARC workstation.

### 2.3. Tests of photocatalytic activity

The photocatalytic activities of the samples were evaluated by the degradation of organic dyes, including methylene blue (MB) and methyl orange (MO), and photocatalytic reduction of Cr(VI) to Cr(III) in an aqueous solution under the irradiation of ultraviolet (UV) light. Typically, a 30 mg portion of catalyst was suspended in 120 mL of 10 ppm dyes or $K_2Cr_2O_7$ solution. Before irradiation, the suspensions were stirred in the dark for 2 h to ensure the establishment of adsorption–desorption equilibrium. Under ambient conditions and stirring, the quartz tube was exposed to the UV light irradiation produced by a 300 W Xe arc lamp (PLS-SXE 300, Beijing Perfectlight Co. Ltd.) with a band-pass light filter (λ = 365 ± 15 nm). A 3 mL sample solution was taken at a certain time interval during the experiment and centrifuged to remove the catalyst completely. The solution was analyzed on a Varian UV–vis spectrophotometer (Cary-50, Varian Co. Ltd). The percentage of degradation of dyes, and reduction of Cr(VI) to Cr(III), is reported as $C/C_0$. Here, $C$ is the concentration of dyes or Cr(VI) solution at each irradiated time interval, while $C_0$ is the initial concentration of dyes or Cr(VI) solution after the adsorption–desorption equilibrium is reached. Controlled photoactivity experiments using different radical scavengers (ammonium oxalate as scavenger for photogenerated holes, $K_2S_2O_8$ as scavenger for electrons, *tert*-butyl alcohol as scavenger for hydroxyl radical species, and benzoquinone as scavenger for superoxide radical species) were performed similar to the above photocatalytic experiments except that the radical scavengers (60 mg) were added to the reaction system.

A recycled photoactivity test on the used catalyst was done as following. Typically, after the reaction of 1st run under UV light irradiation, the liquid and catalyst were separated by centrifugation. The liquid was decanted, while the used catalyst was washed with anhydrous ethanol and deionized water carefully and then dried in an oven. The fresh liquid, namely dye (or $K_2Cr_2O_7$) and solvent deionized water, was mixed with this used catalyst subject to the 2nd run photoactivity testing. In analogy, the recycled 3rd, and 4th photoactivity testing was performed.

## 3. Results and discussion

### 3.1. XRD analysis

Fig. 1 shows the XRD patterns of the as-prepared RGO/ZnO-S1 composites and RGO/ZnO-S2 composites. It is clear to see that the RGO/ZnO-S1 composites and RGO/ZnO-S2 composites with different weight addition ratios of RGO have similar XRD patterns. The peaks of scattering angles 2θ values located at *ca.* 31.8°, 34.4°, 36.3°, 47.5°, 56.6°, 62.9°, 66.4°, 68.0°, 69.1°, 72.6°, and 76.9° can be indexed to (1 0 0), (0 0 2), (1 0 1), (1 0 2), (1 1 0), (1 0 3), (2 0 0), (1 1 2), (2 0 1), (0 0 4), and (2 0 2) facet crystal planes of hexagonal wurtzite ZnO (JCPDS No. 36-1451), respectively [77]. However, there is no apparent peak for the separate RGO in the RGO/ZnO composites to be detected. This can be ascribed to two probable causes. One is the low amount and relatively low diffraction intensity of RGO in the composites of RGO/ZnO [77]. The other is probably due to the disappearance of the layer-stacking regularity after redox of graphite [51].

### 3.2. Optical property

Fig. 2 displays the UV–vis diffuse reflectance spectra (DRS) of RGO/ZnO-S1 composites and RGO/ZnO-S2 composites. It is observed that RGO/ZnO-S1 composites have the similar absorption intensity in the UV region. However, regarding the 20% RGO/ZnO-S2 composite, it should be noted that the higher amount of RGO significantly shields the UV light absorption by ZnO-S2. Furthermore, the presence of RGO leads to the continuous absorption band in the range of 400–800 nm for both RGO/ZnO-S1 and RGO/ZnO-S2 composites. With the increase of RGO content, there is an enhanced absorption in visible light region, which is in agreement with the color change of the samples (Fig. S1 and S2 in the Supporting Information).

### 3.3. Photocatalytic performance

The photocatalytic activity of RGO/ZnO-S1 composites and RGO/ZnO-S2 composites has been evaluated by photocatalytic degradation of two dyes, methylene blue (MB) and methyl orange (MO), which are well-known organic dyes pollutant in wastewater produced from textile and other industrial processes [16,62], and photocatalytic reduction of Cr(VI), which is a well-known heavy metal ions pollutant in wastewater produced from electrolyte and other industrial processes [59]. Blank experiments

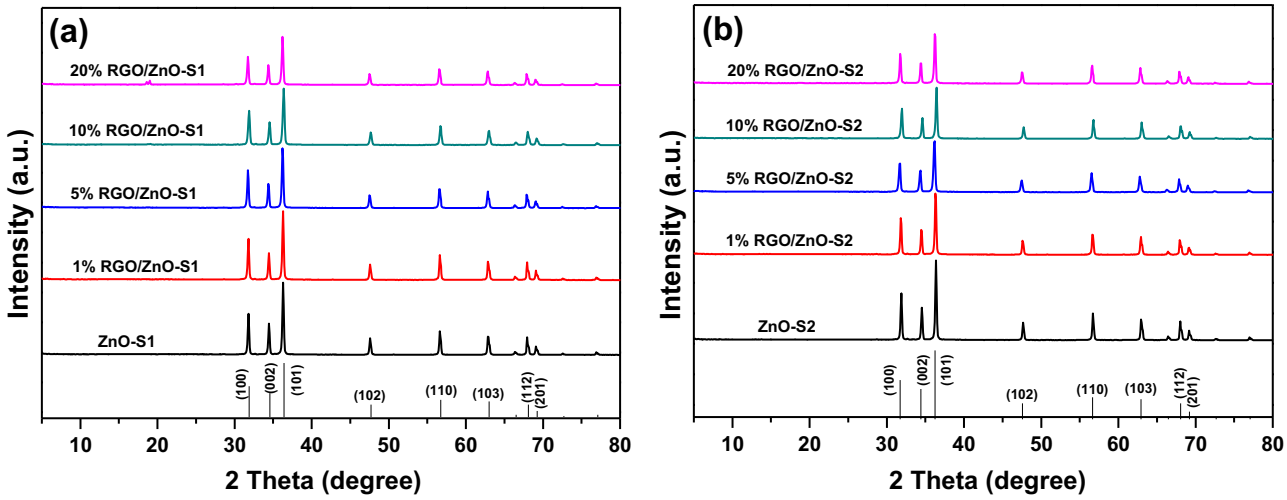


**Fig. 1.** XRD patterns of RGO/ZnO-S1 composites (a) and RGO/ZnO-S2 composites (b).

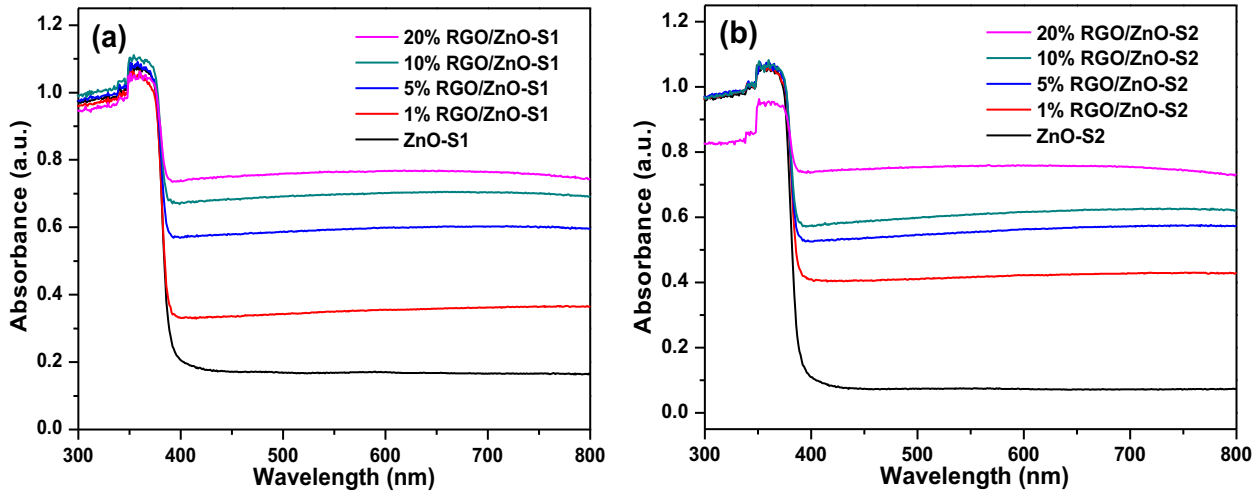


**Fig. 2.** The UV–vis diffuse reflectance spectra (DRS) of RGO/ZnO-S1 composites (a) and RGO/ZnO-S2 composites (b) with different weight ratios.

show that no activity is observed in the absence of catalyst or light irradiation. The controlled blank experiment over the bare RGO also shows no photocatalytic activity for degradation of dyes and reduction of Cr(VI). Fig. 3 illustrates the photocatalytic activity for the degradation of MB under UV light irradiation over the RGO/ZnO-S1 composites and RGO/ZnO-S2 composites. The pseudo-first-order relationship was revealed by the plots of $\ln(C_0/C)$ vs irradiation time ($t$): $\ln(C_0/C) = k_a t$, where

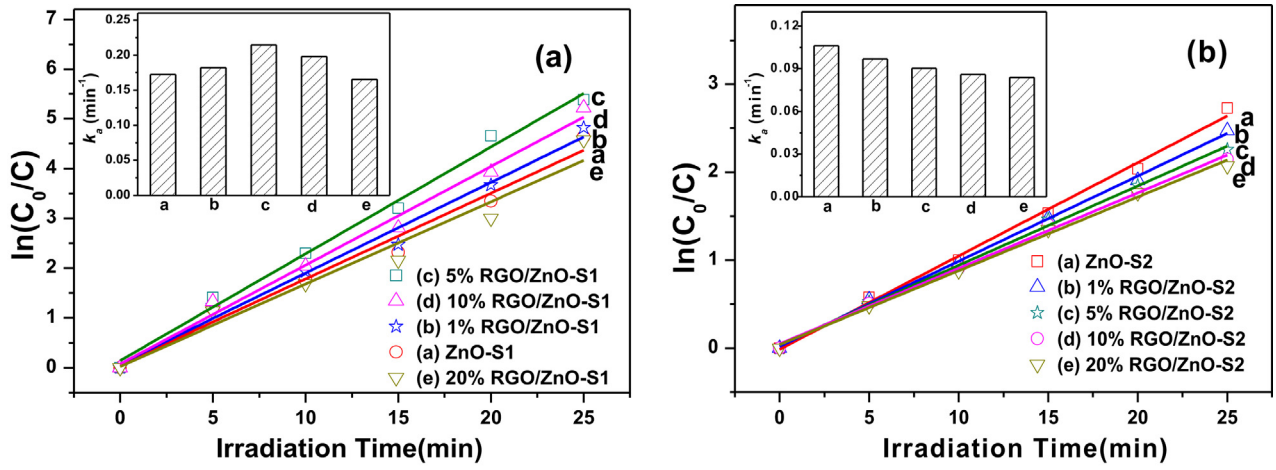


**Fig. 3.** Photocatalytic degradation of methylene blue (MB) over RGO/ZnO-S1 composites (a) and RGO/ZnO-S2 composites (b) under UV light irradiation; inset is the apparent rate constant ($k_a$).

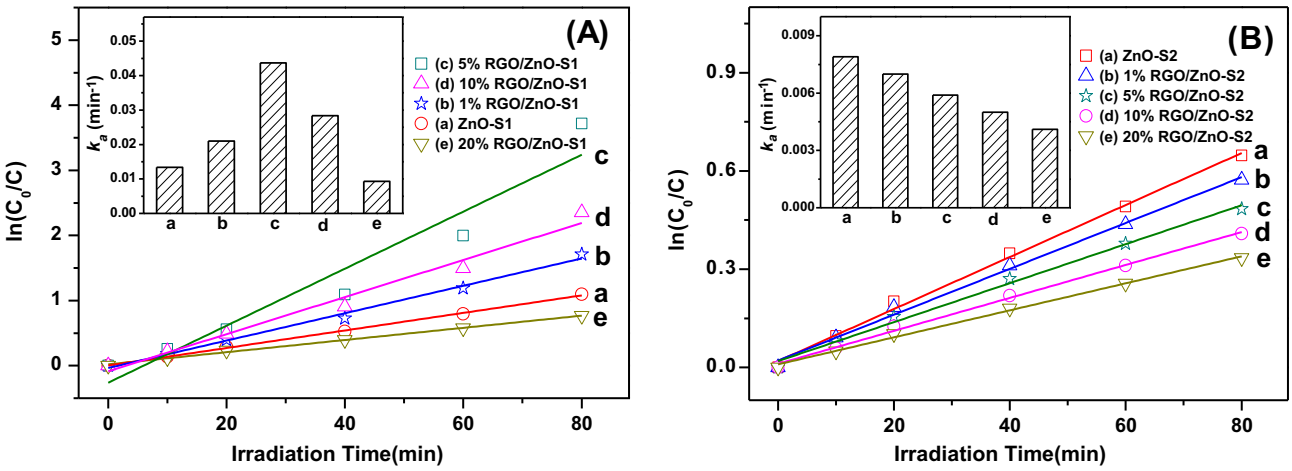


**Fig. 4.** Photocatalytic reduction of Cr(VI) to Cr(III) over RGO/ZnO-S1 composites (a) and RGO/ZnO-S2 composites (b) under UV light irradiation; inset is the apparent rate constant ($k_a$).

$k_a$ is the apparent first-order rate constant. The kinetic rate constants follow the order 5% RGO/ZnO-S1 (0.215 $min^{-1}$) > 10% RGO/ZnO-S1 (0.198 $min^{-1}$) > 1% RGO/ZnO-S1 (0.182 $min^{-1}$) > ZnO-S1 (0.172 $min^{-1}$) > 20% RGO/ZnO-S1 (0.165 $min^{-1}$) > ZnO-S2 (0.106 $min^{-1}$) > 1% RGO/ZnO-S2 (0.0969 $min^{-1}$) > 5% RGO/ZnO-S2 (0.0903 $min^{-1}$) > 10% RGO/ZnO-S2 (0.0859 $min^{-1}$) > 20% RGO/ZnO-S2 (0.0839 $min^{-1}$). Similar photoactivity trend can also be observed for degradation of MO (Fig. S3, Supporting Information). In addition, such an analogous photoactivity trend is also observed for photocatalytic reduction of Cr(VI) to Cr(III). As shown in Fig. 4, with regard to photocatalytic reduction of Cr(VI), the kinetic rate constants follow the order 5% RGO/ZnO-S1 (0.0437 $min^{-1}$) > 10% RGO/ZnO-S1 (0.0284 $min^{-1}$) > 1% RGO/ZnO-S1 (0.0210 $min^{-1}$) > ZnO-S1 (0.0134 $min^{-1}$) > 20% RGO/ZnO-S1 (0.0093 $min^{-1}$) > ZnO-S2 (0.0079 $min^{-1}$) > 1% RGO/ZnO-S2 (0.0070 $min^{-1}$) > 5% RGO/ZnO-S2 (0.0059 $min^{-1}$) > 10% RGO/ZnO-S2 (0.0050 $min^{-1}$) > 20% RGO/ZnO-S2 (0.0041 $min^{-1}$). It is clear that the 5% RGO/ZnO-S1 composite shows the best photocatalytic performance, suggesting the synergy interaction in an appropriate manner between RGO and ZnO plays an important role in enhancing the photoactivity of RGO–ZnO composites. The excess addition of RGO will lower the light intensity through the depth of reaction solution, which consequently decreases the photoactivity, as reflected by the lower rate constant for 20% RGO/ZnO-S1 than that for bare ZnO-S1.

In particular, it should be noted that all the RGO/ZnO-S2 composites with different weight ratios of RGO show lower photoactivity than the bare ZnO-S2, indicating that the size of ZnO particles should play an important role in the synergetic interaction between ZnO and RGO and hence affecting the overall photocatalytic performance of RGO–ZnO composites. In order to shed light on the relationship of structure-photoactivity, we have performed a series of characterizations on the optimum 5% RGO/ZnO-S1 composite with higher photoactivity than bare ZnO-S1 and its analogue 5% RGO/ZnO-S2 with lower photoactivity than bare ZnO-S2.

### 3.4. Morphology

Fig. 5 displays the typical scanning electron microscopy (SEM) images of the optimum 5% RGO/ZnO-S1 composite and its analogue 5% RGO/ZnO-S2 composite. For comparison, the SEM images of bare ZnO-S1 and ZnO-S2 are also given. In addition, the statistical size distribution of ZnO particles in both 5% RGO/ZnO-S1 and 5% RGO/ZnO-S2 has been displayed in Fig. 5b and e. It can be seen clearly that the primary difference between 5% RGO/ZnO-S1 and 5% RGO/ZnO-S2 is that they have different particles size distribution of ZnO. The ZnO particle size is in the range of 20–100 nm for 5% RGO/ZnO-S1, while that for 5% RGO/ZnO-S2 is in the range of 50–500 nm. Correlating the morphology feature by SEM analysis with the above observed photoactivity order, it is evident that the particle size of ZnO directly affects the interfacial contact degree between RGO sheet and ZnO, which in turn influences the photoactivity of RGO–ZnO composites. In other words, there is a relatively good interfacial contact between RGO and ZnO-S1 particles with small size distribution for 5% RGO/ZnO-S1 while the interfacial contact between RGO and ZnO-S2 particles with large size distribution for 5% RGO/ZnO-S2 is relatively poor. Since the transfer of photogenerated electrons from ZnO particles to the RGO sheet occurs across the interface between ZnO and RGO, the degree of interfacial contact plays a key role on the charge carriers transfer for the RGO/ZnO composites under UV light irradiation, which consequently decides the overall photoactivity. Thus, it can be reasonably understood that the 5% RGO/ZnO-S1 composite exhibits enhanced photoactivity than bare ZnO-S1. But, the 5% RGO/ZnO-S2 composite shows decreased photoactivity as compared to bare ZnO-S2. To better understand this standpoint, we have used the photoelectrochemical technique to characterize the samples of bare ZnO-S1, bare ZnO-S2, the optimum 5% RGO/ZnO-S1 and 5% RGO/ZnO-S2 in order to understand the particles size effect on the charge carriers generation and transfer process under UV light irradiation.

### 3.5. Photoelectrochemical and photoluminescence analysis

Fig. 6 shows the photocurrent transient response for the electrodes of 5% RGO/ZnO-S1, 5%RGO/ZnO-S2, bare ZnO-S1 and bare ZnO-S2 upon UV light irradiation. It can be seen that, with the light switched -on and -off cycles, the optimum 5% RGO/ZnO-S1 sample has the highest photocurrent transient response upon UV light irradiation among these four samples, suggesting the remarkably efficient separation of charge carriers, i.e., electron–holes pairs, which is in agreement with the highest photoactivity of 5% RGO/ZnO-S1 toward degradation of dyes and reduction of Cr(VI). It should be noted that the photocurrent transient response over bare ZnO-S2 is higher than 5% RGO/ZnO-S2, which is in line with the lower photoactivity of 5% RGO/ZnO-S2 than bare ZnO-S2. Fig. 7 shows the electrochemical impedance spectroscopy (EIS) Nyquist plots of the electrode samples of 5% RGO/ZnO-S1, 5% RGO/ZnO-S2, bare ZnO-S1 and bare ZnO-S2 upon UV light irradiation, all of which show depressed semicircles. Notably, the introduction of RGO causes significant decrease in the arc for 5% RGO/ZnO-S1 compared

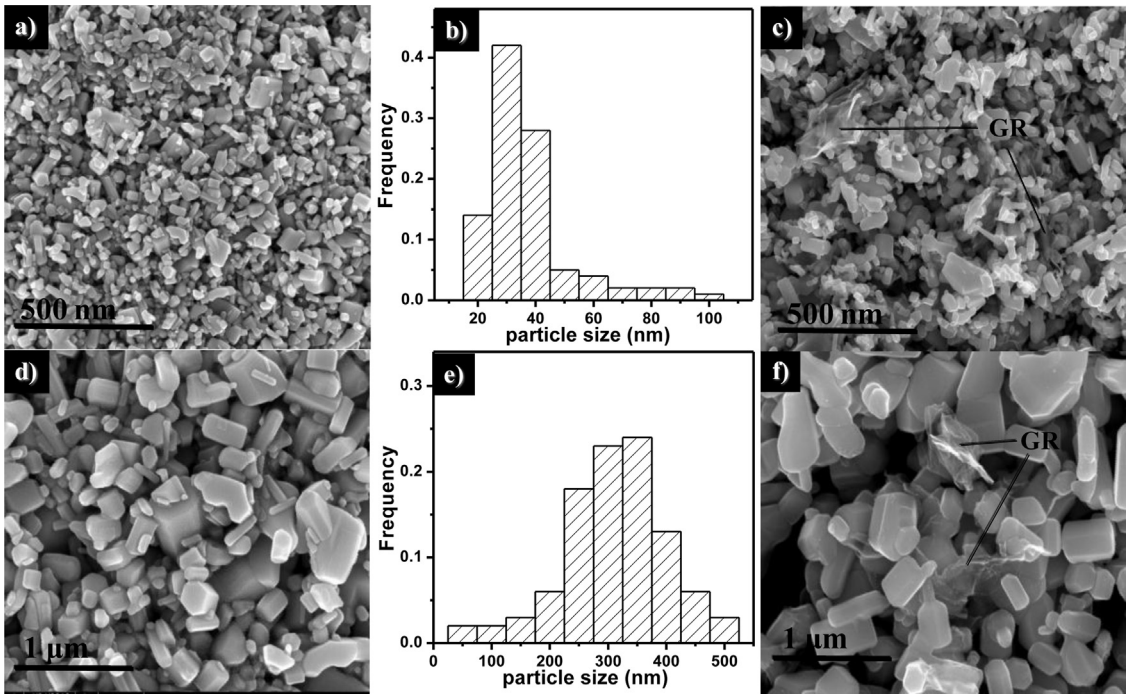


**Fig. 5.** Typical SEM images of bare ZnO-S1 (a), 5%RGO/ZnO-S1 composite (c), bare ZnO-S2 (d) and 5%RGO/ZnO-S2 composite (f); the statistical size distribution of ZnO particles in 5%RGO/ZnO-S1 (b) and in 5% RGO/ZnO-S1 (e).

with other samples, which suggests the more efficient transfer of charge carriers over 5% RGO/ZnO-S1 than that over other samples. The photoluminescence (PL) analysis, as displayed in Fig. S4 (Supporting Information), also evidences that the hybridization of RGO with ZnO particles can retard the recombination of photogenerated charge carriers, i.e., electron–hole pairs, from semiconductor ZnO. Thus, it is clear that 5% RGO/ZnO-S1 with small particles size of ZnO and relatively good interfacial contact can utilize the electron conductivity of RGO sheet more efficiently than that for 5% RGO/ZnO-S2 with large particles size of ZnO and relatively poor interfacial contact.

### 3.6. Photogenerated active radical species

To learn the involvement of active radical species in the photocatalytic process, we have performed the electron spin resonance (ESR) analysis of the samples of 5%RGO/ZnO-S1, 5%RGO/ZnO-S2, bare ZnO-S1 and bare ZnO-S2. Blank experiments show that no signal is observed by ESR analysis in the absence of catalyst or light irradiation. Under the irradiation of UV light, the signal of hydroxyl radicals (•OH) and superoxide radicals ($O_2^{\bullet -}$) for all the samples can be observed, as displayed in Fig. 8. In particular, under the same operational conditions, the 5% RGO/ZnO-S1 composite shows the strongest intensity of •OH and $O_2^{\bullet -}$, which seems consistent with the more efficient separation and transfer of charge carriers from RGO/ZnO-S1 as observed from the above photoelectrochemical analysis.

### 3.7. Photocatalytic mechanism

To further understand the role of primary active species and underlying reaction mechanism involved for degradation of dye MB and reduction of Cr(VI) over the optimum 5%RGO/ZnO-S1 composite under UV light irradiation, we have carried out

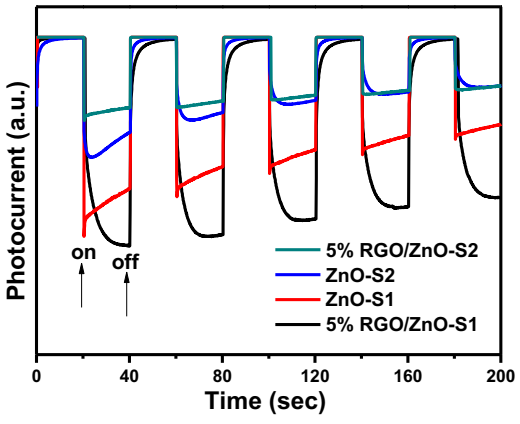


**Fig. 6.** Photocurrent transient response of the sample electrodes of 5%RGO/ZnO-S1 composite, 5%RGO/ZnO-S2 composite, bare ZnO-S1 and bare ZnO-S2 in a 0.2 M $Na_2SO_4$ aqueous solution without bias *versus* the Ag/AgCl electrode under UV light irradiation.

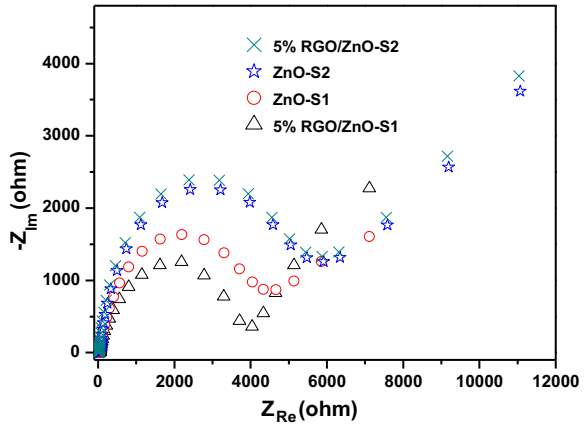


**Fig. 7.** Nyquist impedance plots of the sample electrodes of 5% RGO/ZnO-S1 composite, 5%RGO/ZnO-S2 composite, bare ZnO-S1 and bare ZnO-S2 under UV light irradiation.

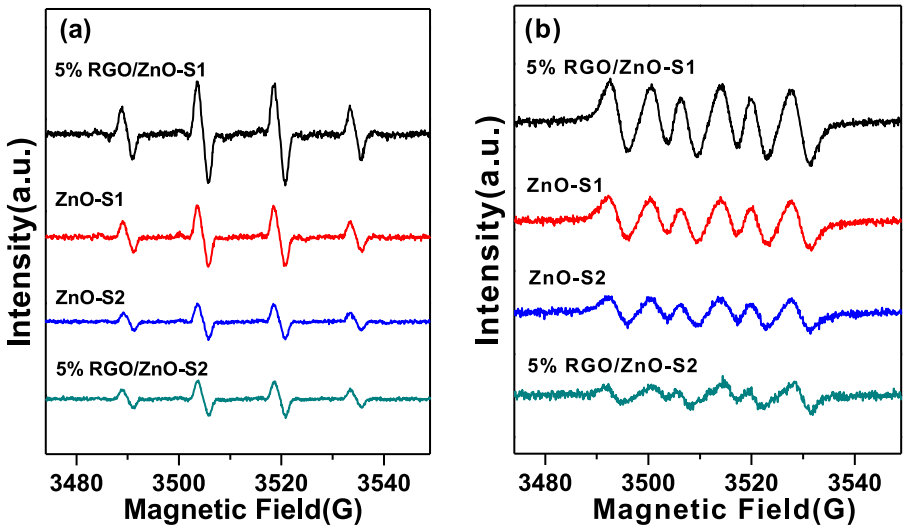


**Fig. 8.** ESR spectra of radical adducts trapped by DMPO over the 5% RGO/ZnO-S1 composite, 5%RGO/ZnO-S2 composite, bare ZnO-S1 and ZnO-S2 dispersions under UV light irradiation; (a) DMPO-•OH formed in irradiated aqueous dispersions; (b) DMPO-$O_2^{\bullet-}$ formed in irradiated methanol dispersions.

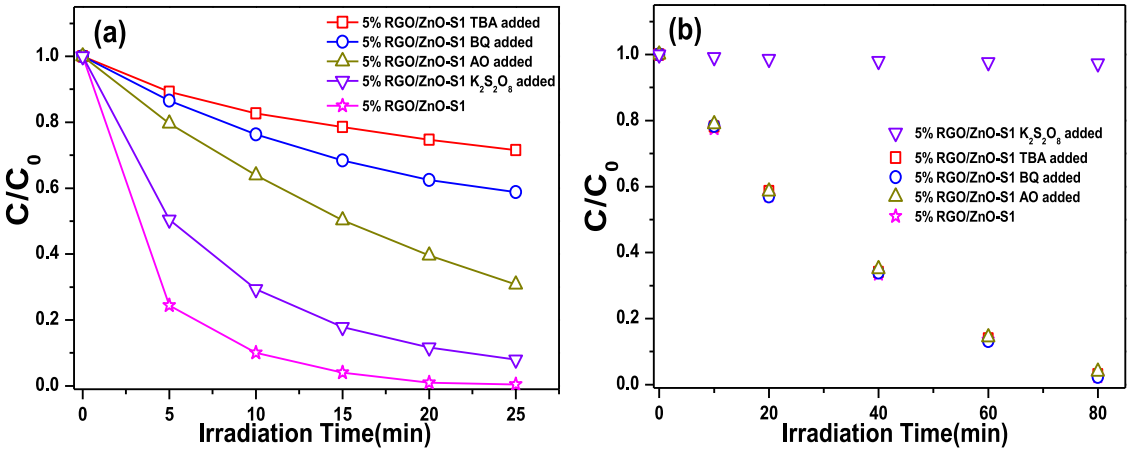


**Fig. 9.** Control experiments using different radical scavengers for the photocatalytic degradation of methylene blue (a) and photocatalytic reduction of Cr(VI) (b) over optimum 5% RGO/ZnO-S1 composite; the reaction in the absence of radical scavengers, reaction with *tert*-butyl alcohol (TBA) as scavenger for hydroxyl radicals, reaction with benzoquinone (BQ) as scavenger for superoxide radicals, reaction with ammonium oxalate (AO) as scavenger for photogenerated holes, and reaction with $K_2S_2O_8$ as scavenger for photogenerated electrons under UV light irradiation.

control experiments with adding scavengers for hydroxyl radicals (•OH), superoxide radicals ($O_2^{\bullet-}$), holes ($h^+$), and electrons ($e^-$), respectively [8,56,83–85]. Fig. 9a shows the photocatalytic activities of 5%RGO/ZnO-S1 for the degradation of MB in the presence of different radical scavengers, i.e., $K_2S_2O_8$ scavenger for electrons, ammonium oxalate (AO) scavenger for holes, benzoquinone (BQ) scavenger for $O_2^{\bullet-}$, and *tert*-butyl alcohol (TBA) scavenger for •OH, respectively. It is obvious that the order of affecting the rate for degradation of MB follows that of $^{\bullet}OH > O_2^{\bullet-} > h^+ > e^-$. Namely, the hydroxyl radicals (•OH) play the most important key role in degradation of MB, and this observation is in agreement with the common viewpoint on photocatalytic degradation of organic dyes over semiconductor [85,86]. However, with regard to photocatalytic reduction of Cr(VI) over 5%RGO/ZnO-S1 under UV light irradiation, the case is quite different, as reflected in Fig. 9b. The adding of TBA, BQ, or AO into the reaction system does not affect the photocatalytic reduction rate of Cr(VI) at all over the 5%RGO/ZnO-S1 composite. Whereas, the adding of $K_2S_2O_8$ scavenger for electrons completely inhibit the photocatalytic reduction of Cr(VI), suggesting that photocatalytic reduction of Cr(VI) is driven by the photogenerated electrons from 5%RGO/ZnO-S1 under UV light irradiation.

Based on the above experiments, a tentative photocatalytic reaction mechanism for degradation of dyes and reduction of Cr (VI) over the RGO/ZnO-S1 composite can be schematically proposed in Fig. 10. Under UV light irradiation, the electron–hole pairs are generated from the semiconductor ZnO. It has been reported that

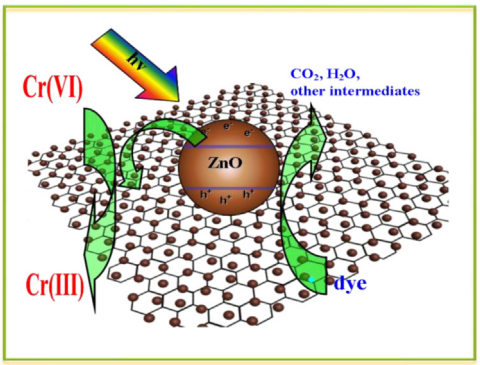


**Fig. 10.** Proposed schematic mechanism for photocatalytic degradation of dyes and reduction of Cr(VI) over RGO/ZnO-S1 composites under UV light irradiation.

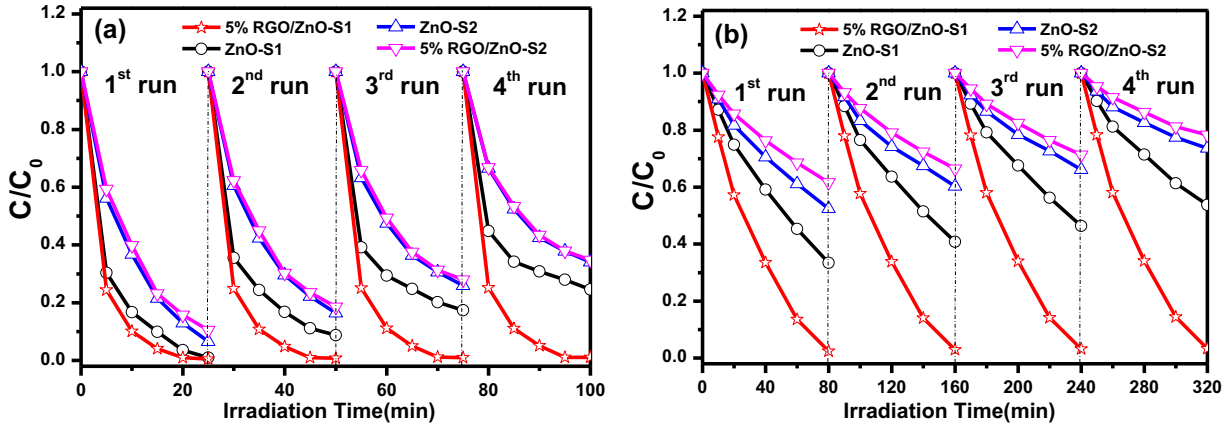


**Fig. 11.** Recycled photoactivity testing of 5%RGO/ZnO-S1 composite, 5%RGO/ZnO-S2 composite, bare ZnO-S1 and bare ZnO-S2 toward degradation of MB (a) and reduction of Cr(VI) to Cr(III) (b) under UV light irradiation.

the calculated Fermi level ($E_F$) of RGO and the conduction band (CB) edge ($E_{CB}$) of ZnO are *ca.* −0.08 and *ca.* −0.36 V versus NHE, respectively [42,52]. Thus, the photogenerated electrons from ZnO can transfer to the RGO sheet, thereby enhancing the lifetime and transfer of electron–hole pairs, which is evidenced by the above photoelectrochemical and photoluminescence analysis. This consequently contributes to increasing the overall photoactivity. For photocatalytic reduction of Cr(VI), only photogenerated electrons are the primary active species. Whereas, for photocatalytic degradation of dye MB, the superoxide radicals ($O_2^{\bullet-}$), holes, hydroxyl radicals ($^{\bullet}OH$) and photogenerated electrons together play synergistic effects.

### 3.8. Photocatalyst recycling and photostability

To evaluate the photostability of optimum 5%RGO/ZnO-S1, 5%RGO/ZnO-S2, bare ZnO-S1 and bare ZnO-S2, the recycled experiments for photocatalytic degradation of MB and reduction of Cr(VI) have been performed, and the results are shown in Fig. 11. It is interesting to observe that the 5%RGO/ZnO-S1 composite exhibits relatively stable photocatalytic activity while the obvious photocorrosion, i.e., photoactivity loss during the recycled experiments, is observed for bare ZnO-S1, bare ZnO-S2 and 5% RGO/ZnO-S2. During the recycled experiments for four times, it is striking to find that the photocatalyst of 5%RGO/ZnO-S1 shows almost no deactivation while the photocorrosion phenomenon can still be observed for 5%RGO/ZnO-S2. In order to probe the difference of the interaction between RGO and ZnO, we have performed the Fourier transformed infrared spectroscopy (FT-IR) of these four samples as shown in Fig. 12. For the optimum 5% RGO/ZnO-S1 and its analog 5%RGO/ZnO-S2, the broad absorption at low frequency (below 700 $cm^{-1}$) can be attributed to the vibration of Zn—O bonds in ZnO, similar to that in the spectrum of bare ZnO-S1 and bare ZnO-S2. The absorption band appearing at *ca.* 1600 $cm^{-1}$ shows the skeletal vibration of the RGO sheets. In particular, it should be noticed that a specific absorption band, appearing at *ca.* 1408 $cm^{-1}$, has been observed for only 5%RGO/ZnO-S1. This peak could be ascribed to the vibration of the C—O bonds formed between RGO and ZnO-S1. Such a hybridization interaction between ZnO-S1 and RGO with a π-conjugative 2D system could reduce the activation of surface oxygen atom of ZnO-S1, by which the photocorrosion of ZnO-S1 is significantly inhibited. Indeed, this analogous phenomenon has also been observed in a previous report on $C_{60}$-ZnO composites photocatalysts [30]. In contrast, such a chemical bond is not observed for the hybridization in the RGO/ZnO-S2 composite. Thus, it can be reasonably concluded that the relatively small particles size of ZnO-S1 in 5%RGO/ZnO-S1 leads to the more interfacial interaction between RGO and ZnO whereas the relatively large particle size of ZnO-S2 in 5%RGO/ZnO-S2 causes the less efficient interfacial interaction. This consequently leads to the decreased photoactivity of 5%RGO/ZnO-S2 as compared to bare ZnO-S2 while simultaneously the photocorrosion of 5%RGO/ZnO-S2 can still be observed. Therefore, in order to achieve an efficient RGO-semiconductor photocatalyst, it is of key importance to control the composition ratio and the semiconductor particle size to achieve an optimal synergy effect between RGO and semiconductor, by which the electron conductivity of GR can be really utilized to increase the lifetime of electron–hole pairs photogenerated from semiconductor.

Thus far, important information based on the present work can be proposed as the following. The simple "hard" integration of solid ZnO particles with RGO provides us with a reasonable basis to study the particle size effect of ZnO on the photoactivity of RGO/ZnO composites, although this synthesis approach is not able to utilize the surfactant-like structure-directing role of GO for water-soluble precursor of semiconductor, instead of solid semiconductor particles, in the solution phase [54]. The smaller particle size of semiconductor ZnO-S1 contributes to the increased interfacial interaction between ZnO-S1 and RGO, which leads to the enhanced photoactivity and anti-photocorrosion for degradation of dyes and reduction of heavy metal ion, Cr (VI). On the contrary, because ZnO-S2 has the relatively larger particle size, the interfacial interaction between

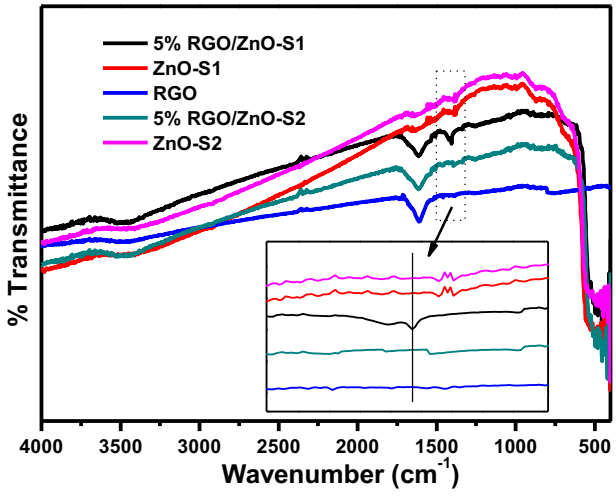


**Fig. 12.** Fourier transformed infrared spectroscopy (FT-IR) spectra of 5%RGO/ZnO-S1 composite, 5%RGO/ZnO-S2 composite, bare ZnO-S1, bare ZnO-S2 and RGO.

ZnO-S2 and RGO is poor; in this case, the hybridization of ZnO-S2 with RGO will lower the photoactivity because the electron conductivity of RGO can not be utilized efficiently to boost the fate and transfer of charge carriers photogenerated from ZnO-S2 under UV light irradiation.

## 4. Conclusion

In summary, a series of RGO/ZnO-S1 and RGO/ZnO-S2 composites with different weight addition ratios of RGO have been fabricated via a facile solvothermal method. It is found that the RGO/ZnO-S1 composite with the ZnO particles size of 20–100 nm exhibits the enhanced photocatalytic activity, but RGO/ZnO-S2 composite with the ZnO particles size of 50–500 nm shows decreased photocatalytic activity toward both degradation of dye MB and reduction of Cr(VI). It is found that ZnO-S1, with relatively small particles size distribution, is able to hybridize with RGO sheet more efficiently than that for the hybridization of ZnO-S2, with large particles size distribution, with RGO sheet. Such a particle size effect leads the more efficient interfacial interaction between ZnO-S1 and RGO, which leads to both the enhanced photoactivity and the decreased photocorrosion. In addition, we have also used the radicals scavengers technique to study the role of photoactive species involved in the photocatalytic degradation of MB and reduction of Cr(VI). It is expected that this current research could promote further interest on synthesizing efficient GR-semiconductor photocatalysts for environment remediation.

## Acknowledgements

The support by the National Natural Science Foundation of China (NSFC) (21173045, 20903023), the Award Program for Minjiang Scholar Professorship, the Natural Science Foundation (NSF) of Fujian Province for Distinguished Young Investigator Grant (2012J06003), Program for Changjiang Scholars and Innovative Research Team in Universities (PCSIRT0818), Program for Returned High-Level Overseas Chinese Scholars of Fujian Province, and the Project Sponsored by the Scientific Research Foundation for the Returned Overseas Chinese Scholars, State Education Ministry, is gratefully acknowledged.

## Appendix A. Supplementary data

Supplementary data associated with this article can be found, in the online version, at http://dx.doi.org/10.1016/j.apcatb.2013.04.059.

## References

[1] N. Serpone, A.V. Emeline, Journal of Physical Chemistry Letters 3 (2012) 673–677.
[2] K. Maeda, K. Domen, Journal of Physical Chemistry Letters 1 (2010) 2655–2661.
[3] A. Kubacka, M. Fernandez-Garcia, G. Colon, Chemical Reviews 112 (2012) 1555–1614.
[4] P.V. Kamat, Journal of Physical Chemistry C 111 (2007) 2834–2860.
[5] N. Zhang, S. Liu, Y.-J. Xu, Nanoscale 4 (2012) 2227–2238.
[6] N. Zhang, Y. Zhang, X. Pan, X. Fu, Y.-J. Xu, Science China Chemistry 41 (2011) 1097–1111.
[7] Y. Zhuang, H.Y. Song, G. Li, Y.-J. Xu, Materials Letters 64 (2010) 2491–2493.
[8] Y. Zhang, N. Zhang, Z.-R. Tang, Y.-J. Xu, Chemical Science 3 (2012) 2812–2822.
[9] Z.-R. Tang, F. Li, Y. Zhang, X. Fu, Y.-J. Xu, Journal of Physical Chemistry C 115 (2011) 7880–7886.
[10] Z.-R. Tang, Y. Zhang, Y.-J. Xu, RSC Advances 1 (2011) 1772–1777.
[11] Z.-R. Tang, Y. Zhang, Y.-J. Xu, ACS Applied Materials & Interfaces 4 (2012) 1512–1520.
[12] H. Cheng, B. Huang, Y. Liu, Z. Wang, X. Qin, X. Zhang, Y. Dai, Chemical Communications 48 (2012) 9729–9731.
[13] X. Liu, L. Pan, T. Lv, G. Zhu, Z. Sun, C. Sun, Chemical Communications 47 (2011) 11984–11986.
[14] K. Imamura, K. Hashimoto, H. Kominami, Chemical Communications 48 (2012) 4356–4358.
[15] N. Zhang, X. Fu, Y.-J. Xu, Journal of Materials Chemistry 21 (2011) 8152–8158.
[16] Y.-J. Xu, Y. Zhuang, X. Fu, Journal of Physical Chemistry C 114 (2010) 2669–2676.
[17] Y. Zhang, Z.-R. Tang, X. Fu, Y.-J. Xu, Applied Catalysis B 106 (2011) 445–452.
[18] X. Chen, S. Shen, L. Guo, S.S. Mao, Chemical Reviews 110 (2010) 6503–6570.
[19] R. Georgekutty, M.K. Seery, S.C. Pillai, Journal of Physical Chemistry C 112 (2008) 13563–13570.
[20] L. Huang, S.P. Lau, H.Y. Yang, E.S.P. Leong, S.F. Yu, Journal of Physical Chemistry B 109 (2005) 7746–7748.
[21] H. Zeng, W. Cai, P. Liu, X. Xu, H. Zhou, C. Klingshirn, H. Kalt, ACS Nano 2 (2008) 1661–1670.
[22] Y. Li, W. Xie, X. Hu, G. Shen, X. Zhou, Y. Xiang, X. Zhao, P. Fang, Langmuir 26 (2010) 591–597.
[23] C.A.K. Gouvea, F. Wypych, S.G. Moraes, N. Duran, N. Nagata, P. Peralta-Zamora, Chemosphere 40 (2000) 433–440.
[24] C. Ye, Y. Bando, G. Shen, D. Golberg, Journal of Physical Chemistry B 110 (2006) 15146–15151.
[25] R. Comparelli, E. Fanizza, M.L. Curri, P.D. Cozzoli, G. Mascolo, A. Agostiano, Applied Catalysis B 60 (2005) 1–11.
[26] F. Xiao, ACS Applied Materials & Interfaces 4 (2012) 7055–7063.
[27] Y. Li, X. Zhou, X. Hu, X. Zhao, P. Fang, Journal of Physical Chemistry C 113 (2009) 16188–16192.
[28] L. Zhang, H. Cheng, R. Zong, Y. Zhu, Journal of Physical Chemistry C 113 (2009) 2368–2374.
[29] H. Zhang, R. Zong, Y. Zhu, Journal of Physical Chemistry C 113 (2009) 4605–4611.
[30] H. Fu, T. Xu, S. Zhu, Y. Zhu, Environmental Science and Technology 42 (2008) 8064–8069.
[31] N. Zhang, Y. Zhang, Y.-J. Xu, Nanoscale 4 (2012) 5792–5813.
[32] Q. Xiang, J. Yu, M. Jaroniec, Chemical Society Reviews 41 (2012) 782–796.
[33] I.V. Lightcap, T.H. Kosel, P.V. Kamat, Nano Letters 10 (2010) 577–583.
[34] Q. Xiang, J. Yu, M. Jaroniec, Journal of the American Chemical Society 134 (2012) 6575–6578.
[35] Q. Xiang, J. Yu, M. Jaroniec, Journal of Physical Chemistry C 115 (2011) 7355–7363.
[36] P.V. Kamat, Journal of Physical Chemistry Letters 2 (2011) 242–251.
[37] W. Fan, Q. Lai, Q. Zhang, Y. Wang, Journal of Physical Chemistry C 115 (2011) 10694–10701.
[38] L. Han, P. Wang, S. Dong, Nanoscale 4 (2012) 5814–5825.
[39] H. Zhang, X. Lv, Y. Li, Y. Wang, J. Li, ACS Nano 4 (2010) 380–386.
[40] J. Zhang, Z. Xiong, X.S. Zhao, Journal of Materials Chemistry 21 (2011) 3634–3640.
[41] Q.-P. Luo, X.-Y. Yu, B.-X. Lei, H.-Y. Chen, D.-B. Kuang, C.-Y. Su, Journal of Physical Chemistry C 116 (2012) 8111–8117.
[42] T. Xu, L. Zhang, H. Cheng, Y. Zhu, Applied Catalysis B 101 (2011) 382–387.
[43] X. An, J.C. Yu, Y. Wang, Y. Hu, X. Yu, G. Zhang, Journal of Materials Chemistry 22 (2012) 8525–8531.
[44] H. Seema, K.C. Kemp, V. Chandra, K.S. Kim, Nanotechnology 23 (2012) 355705.
[45] Y. Sun, B. Qu, Q. Liu, S. Gao, Z. Yan, W. Yan, B. Pan, S. Wei, Y. Xie, Nanoscale 4 (2012) 3761–3767.
[46] Y.-L. Min, K. Zhang, Y.-C. Chen, Y.-G. Zhang, Separation and Purification Technology 86 (2012) 98–105.
[47] H. Hu, X. Wang, F. Liu, J. Wang, C. Xu, Synthetic Metals 161 (2011) 404–410.
[48] L.L. Zhang, Z. Xiong, X.S. Zhao, ACS Nano 4 (2010) 7030–7036.
[49] Z. Xiong, L.L. Zhang, J. Ma, X.S. Zhao, Chemical Communications 46 (2010) 6099–6101.
[50] Y. Fu, X. Wang, Industrial and Engineering Chemistry Research 50 (2011) 7210–7218.
[51] N. Zhang, Y. Zhang, X. Pan, X. Fu, S. Liu, Y.-J. Xu, Journal of Physical Chemistry C 115 (2011) 23501–23511.
[52] N. Zhang, Y. Zhang, X. Pan, M.-Q. Yang, Y.-J. Xu, Journal of Physical Chemistry C 116 (2012) 18023–18031.
[53] Y. Zhang, Z.-R. Tang, X. Fu, Y.-J. Xu, ACS Nano 4 (2010) 7303–7314.
[54] Y. Zhang, Z.-R. Tang, X. Fu, Y.-J. Xu, ACS Nano 5 (2011) 7426–7435.
[55] Y. Zhang, N. Zhang, Z.-R. Tang, Y.-J. Xu, Physical Chemistry Chemical Physics 14 (2012) 9167–9175.
[56] Y. Zhang, N. Zhang, Z.-R. Tang, Y.-J. Xu, ACS Nano 6 (2012) 9777–9789.
[57] J. Wang, T. Tsuzuki, B. Tang, X. Hou, L. Sun, X. Wang, ACS Applied Materials & Interfaces 4 (2012) 3084–3090.
[58] Y. Yang, L. Ren, C. Zhang, S. Huang, T. Liu, ACS Applied Materials & Interfaces 3 (2011) 2779–2785.
[59] X. Liu, L. Pan, T. Lv, T. Lu, G. Zhu, Z. Sun, C. Sun, Catalysis Science and Technology 1 (2011) 1189–1193.
[60] D. Fu, G. Han, Y. Chang, J. Dang, Materials Chemistry and Physics 132 (2012) 673–681.
[61] T. Kavitha, A.I. Gopalan, W.P. Lee, S.Y. Park, Carbon 50 (2012) 2994–3000.
[62] B. Li, T. Liu, Y. Wang, Z. Wang, Journal of Colloid and Interface Science 509 (2012) 10086–10091.
[63] X. Liu, L. Pan, Q. Zhao, T. Lv, G. Zhu, T. Chen, T. Lu, Z. Sun, C. Sun, Chemical Engineering Journal 183 (2012) 238–243.
[64] T. Lv, L. Pan, X. Liu, T. Lu, G. Zhu, Z. Sun, Journal of Alloys and Compounds 509 (2011) 10086–10091.
[65] X. Chen, Y. He, Q. Zhang, L. Li, D. Hu, T. Yin, Journal of Materials Science 45 (2010) 953–960.
[66] B. Li, H. Cao, Journal of Materials Chemistry 21 (2011) 3346–3349.

[67] H. Fan, X. Zhao, J. Yang, X. Shan, L. Yang, Y. Zhang, X. Li, M. Gao, Catalysis Communications 29 (2012) 29–34.
[68] H.R. Pant, C.H. Park, P. Pokharel, L.D. Tijing, D.S. Lee, C.S. Kim, Powder Technology 235 (2013) 853–858.
[69] B. Saravanakumar, R. Mohan, S.J. Kim, Materials Research Bulletin 48 (2013) 878–883.
[70] Y. Liu, Y. Hu, M. Zhou, H. Qian, X. Hu, Applied Catalysis B 125 (2012) 425–431.
[71] X. Zhou, T. Shi, H. Zhou, Applied Surface Science 258 (2012) 6204–6211.
[72] T. Lv, L. Pan, X. Liu, Z. Sun, Catalysis Science and Technology 2 (2012) 2297–2301.
[73] Q. Zhang, C. Tian, A. Wu, T. Tan, L. Sun, L. Wang, H. Fu, Journal of Materials Chemistry 22 (2012) 11778–11784.
[74] O. Akhavan, Carbon 49 (2011) 11–18.
[75] Y.L. Min, K. Zhang, L.H. Chen, Y.C. Chen, Y.G. Zhang, Diamond & Related Materials 26 (2012) 32–38.
[76] J.M. Lee, Y.B. Pyun, J. Yi, J.W. Choung, W.I. Park, Journal of Physical Chemistry C 113 (2009) 19134–19138.
[77] Y.L. Chen, Z.A. Hu, Y.Q. Chang, H.W. Wang, Z.Y. Zhang, Y.Y. Yang, H.Y. Wu, Journal of Physical Chemistry C 115 (2011) 2563–2571.
[78] H. Chang, Z. Sun, K.Y.F. Ho, X. Tao, F. Yan, W.M. Kwok, Z. Zheng, Nanoscale 3 (2011) 258–264.
[79] Z. Yin, S. Wu, X. Zhou, X. Huang, Q. Zhang, F. Boey, H. Zhang, Small 6 (2010) 307–312.
[80] M. Dutta, S. Sarkar, T. Ghosh, D. Basak, Journal of Physical Chemistry C 116 (2012) 20127–20131.
[81] H. Park, S. Chang, J. Jean, J.J. Cheng, P.T. Araujo, M. Wang, M.G. Bawendi, M.S. Dresselhaus, V. Bulovic, J. Kong, S. Gradecak, Nano Letters 13 (2013) 233–239.
[82] C. Nethravathi, M. Rajamathi, Carbon 46 (2008) 1994–1998.
[83] W. Li, D. Li, Y. Lin, P. Wang, W. Chen, X. Fu, Y. Shao, Journal of Physical Chemistry C 116 (2012) 3552–3560.
[84] A. Syoufian, K. Nakashima, Journal of Colloid and Interface Science 313 (2007) 213–218.
[85] N. Zhang, S. Liu, X. Fu, Y.-J. Xu, Journal of Physical Chemistry C 115 (2011) 9136–9145.
[86] K. Rajeshwar, M.E. Osugi, C.R. Chenthamarakshan, M.V.B. Zanoni, P. Kajitvichyanukul, R. Krishnan-Ayer, Journal of Photochemistry and Photobiology C 9 (2008) 171–192.